Mirrorless optical parametric oscillator inside an all-optical waveguide

Sushree S. Sahoo,* Snigdha S. Pati, and Ashok K. Mohapatra†
School of Physical Sciences, National Institute of Science Education and Research Bhubaneswar, Homi Bhabha National Institute, Jatni-752050, India

(Received 1 May 2018; published 26 December 2018)

Mirrorless optical parametric oscillator (MOPO) is a consequence of intrinsic feedback provided by the nonlinearity in a medium due to the interaction of a pair of strong counterpropagating fields. As the name suggests, the device does not require a cavity for lasing other than the nonlinear medium. Here we report the demonstration of MOPO under the effect of an all-optical waveguide. The efficient four-wave mixing process due to counterpropagating pump and control fields interacting with a multilevel atomic system facilitates the generation of mirrorless Stokes and anti-Stokes fields counterpropagating to each other. The maximum generated laser power could rise up to mW with pump conversion efficiency more than 30%. Furthermore, the cross-phase modulation due to the strong fields creates all-optical waveguides for the generated fields and hence induces correlated spatial modes in the Stokes and the anti-Stokes fields.

DOI: 10.1103/PhysRevA.98.063838

I. INTRODUCTION

MOPO has attracted a lot of attention ever since the phenomenon was first theoretically predicted by Harris [1]. It was experimentally demonstrated for the case of parametric down-conversion in a quasi-phase-matched nonlinear $\chi^{(2)}$ medium [2] and was followed by extensive studies on the coherence properties and conversion efficiency of the phenomenon [3–5]. For the case of $\chi^{(3)}$ medium, two counterpropagating strong driving fields result in the spontaneous generation of biphotons, i.e., Stokes and anti-Stokes field from noise. The photon pairs being generated in opposite directions establish a distributed feedback mechanism assisted by efficient four-wave mixing (FWM). The FWM-based MOPO has been experimentally achieved using electromagnetically induced transparency (EIT) [6] and further has been used to generate narrow-band biphotons [7,8] in cold atomic ensemble. The works by Balic *et al.* [9] and Pavel [10] described the theory of the counterpropagating biphoton generation showing a good agreement with the experimental results. A recent study in cold atomic ensemble includes the transition of photon correlation properties from the biphoton quantum regime to MOPO regime [11]. MOPO in thermal atomic vapor has also been a subject of intensive study. Earlier it was used to investigate optical instabilities and self-oscillation by atomic-vapor degenerate FWM [12–15]. Along with the experimental demonstration of MOPO in thermal atomic vapor for the case of nondegenerate FWM [16], there has been many theoretical studies on the generated photon pairs [17–21]. The phenomenon has also been reported for the Raman process in hot atomic vapor [22].

On the other hand, the nonlinear interaction of a strong beam with medium results in a spatially varying refractive index and hence leads to the formation of an all-optical waveguide. This causes the modification of the spatial profile of a weak probe beam while propagating through the medium. There have been reports on induced focusing [23], spatial-soliton-induced waveguides [24,25], transverse localization [26–28], and EIT-induced waveguides [29–31]. Optically written waveguides in a thermal rubidium vapor cell have been achieved using Gaussian [32] as well as doughnut-shaped pump beams [33,34].

In this work, we demonstrate MOPO in thermal vapor with counterpropagating strong driving fields called as pump and control beams. The Gaussian profiles of the strong fields result in a nonlinear refractive index-induced waveguide for the generated fields and hence leads to the generation of guided single spatiotemporal modes. Although there have been substantial works on the subject of FWM-based MOPO, the spatial modes of the generated fields have not been investigated before. We report an experimental demonstration of the spatial correlation between the fields generated via the MOPO process with a very high pump conversion efficiency. We show that the excitation of the higher order Laguerre-Gauss modes in the generated fields is a result of all-optical waveguides induced by the input Gaussian driving fields unlike for the cases of FWM inside a fiber [35,36] or FWM with input beams containing orbital angular momentum [37,38].

This paper is organized as follows: In Sec. II, we present the theoretical model for the estimation of the cross phase modulation (XPM) experienced by the generated fields as well as for the propagation equations leading to the all optical waveguiding of the generated fields in the system. In Sec. III, we present the experimental methods followed by the experimental study of single spatial mode of the MOPO in Sec. IV.

II. THEORETICAL MODEL

The schematic of the laser configuration and the relevant energy level diagram for MOPO are shown in Fig. 1. A pump laser field with Rabi frequency Ω_p, optical frequency

*sushree.ss@niser.ac.in
†a.mohapatra@niser.ac.in

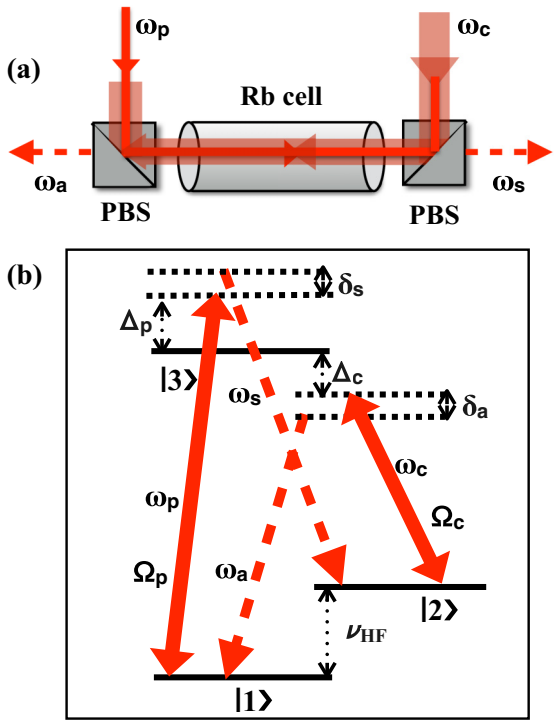

FIG. 1. (a) Schematic of laser configuration for MOPO in thermal vapor, PBS: polarizing beam splitter. (b) Energy level diagram showing the coupling of pump and control laser fields (solid lines) and the generated Stokes and anti-Stokes fields (dashed lines).

ω_p, and detuning Δ_p interacts with the atomic transition $|1\rangle \longrightarrow |3\rangle$. Similarly, the control laser field with Rabi frequency Ω_c, optical frequency ω_c and detuning Δ_c interacts with the atomic transition $|2\rangle \longrightarrow |3\rangle$. The pump and control fields counterpropagate with each other through the atomic medium. The Stokes and the anti-Stokes fields with respective optical frequencies ω_s and ω_a are spontaneously generated and amplified due to nondegenerate FWM process in the medium [6]. With the counterpropagating pump and control beams, the phase-matching condition results in the Stokes and anti-Stokes beams copropagating with the pump and the control fields, respectively. The respective two-photon detunings for the Stokes and the anti-Stokes beams are given by the expressions $\delta_s = \omega_s - \omega_p - \Delta_{\rm LS} + \nu_{\rm HF}$ and $\delta_a = \omega_a - \omega_c + \Delta_{\rm LS} - \nu_{\rm HF}$ with $\Delta_{\rm LS} = \frac{\Omega_p^2}{4\Delta_p} - \frac{\Omega_c^2}{4\Delta_c}$ being the light shift due to the pump and control fields and $\nu_{\rm HF}$ being the splitting of the hyperfine ground states $|1\rangle$ and $|2\rangle$. The energy conservation associated with the FWM process, i.e., $\omega_s + \omega_a = \omega_p + \omega_c$ ensures that $\delta_s + \delta_a = 0$.

A. XPM of the generated fields due to the pump and the control fields

To calculate the XPM experienced by the generated fields in the system, we present a model by considering a system of three levels interacting with a pump and a probe fields while the contribution of the control field is implemented by modification in the equillibirium populations. Here one of the generated beams of the MOPO process is considered as the probe field with Rabi frequency Ω_e and the effect of the other generated field is neglected by considering it to be weak. The pump and control beams are counterpropagating and the direction of the probe field is chosen according to whether it signifies the Stokes field or the anti-Stokes field. The single-photon detunings for the pump, control, and probe fields are given by Δ_p, Δ_c, and Δ_e, whereas Δ is defined by $\Delta_e - \Delta_p$ and is related to δ_s and δ_a by $\Delta = \delta_s - \Delta_{LS} = -(\delta_a + \Delta_{LS})$, as shown in Fig. 1(b). A similar system has been analyzed both theoretically and experimentally to study the narrow absorptive resonance with gain as well as the dispersion of the probe beam [39,40]. The same system has further been used for optical steering, cloning, and splitting of probe beam [41].

Here with the semiclassical approach and rotating-wave approximation, the Hamiltonian of the three level system with the pump and the probe fields is given by

$$\tilde{H} = -\frac{\hbar}{2}\begin{pmatrix} 0 & \Omega_e & 0 \\ \Omega_e^* & -2\Delta_p & \Omega_p \\ 0 & \Omega_p^* & -2\Delta \end{pmatrix}.$$

The time evolution of the system is described by the master equation as

$$i\hbar\frac{d\hat{\rho}}{dt} = [H, \hat{\rho}] + i\hbar\mathcal{L}_D, \tag{1}$$

with

$$\mathcal{L}_D = \begin{pmatrix} \Gamma\rho_{33} & -\gamma_c\rho_{12} & -\Gamma/2\rho_{13} \\ -\gamma_c\rho_{21} & \Gamma\rho_{33} & -\Gamma/2\rho_{23} \\ -\Gamma/2\rho_{31} & -\Gamma/2\rho_{32} & -2\Gamma\rho_{33} \end{pmatrix}.$$

Here $\hat{\rho}$ stands for the density matrix operator and $\mathcal{L}_D$ stands for the Linblad operator, which describes all the decay and dephasing rates in the medium. $\Gamma = 6$ MHz is the population decay rate from the excited state to the ground states. $\gamma_c \sim 1$ MHz is the dephasing rate of the dipoles associated with the ground states, which is dominated by the transit time of the thermal atoms through the beams.

The optical Bloch equations of the density matrix elements are solved in steady state by considering the equilibrium populations of the ground states in the presence of the strong pump and control fields. Since the population decay rates to both the ground states are the same, the population distribution in the hyperfine states depends only on the optical pumping rates due to both the strong fields. Hence the value of $(\rho_{11}^{(\rm eq)} - \rho_{22}^{(\rm eq)})$ is calculated by using $\frac{\rho_{11}^{(\rm eq)}}{\rho_{22}^{(\rm eq)}} = \frac{\Omega_c^2}{\Omega_p^2}\left(\frac{2\Omega_p^2+4\Delta_p^2+\Gamma^2}{2\Omega_c^2+4\Delta_c^2+\Gamma^2}\right)$, as derived by considering the two-level optical pumping rates of the pump and the control fields.

Considering the Doppler broadening in the medium, the laser detunings Δ_p, Δ_c, and Δ_e are modified as $\Delta_p - k_p v$, $\Delta_c + k_c v$ and $\Delta_e - k_e v$, respectively, where v is the velocity and k_p, k_c, k_e are the wave vectors of the pump, control, and probe fields, respectively. With this effect, the nonlinear susceptibility of the weak probe beam due to XPM, $\chi_{\rm XPM}^{(\rm eff)}$, evaluated under the steady-state condition is Doppler-averaged to get, $\chi_{\rm XPM}^{(\rm eff)} = \frac{1}{\sqrt{2\pi}v_p}\left(\frac{2N\mu^2}{\epsilon_0\hbar\Omega_e}\right)\int_{-\infty}^{\infty}\rho_{32}(v)e^{-v^2/2v_p^2}dv$ with v_p being the most probable speed of the atoms, N being the number density, and μ being the atomic dipole moment. The imaginary part of the Doppler-averaged susceptibility provides information about the nonlinear gain or absorption

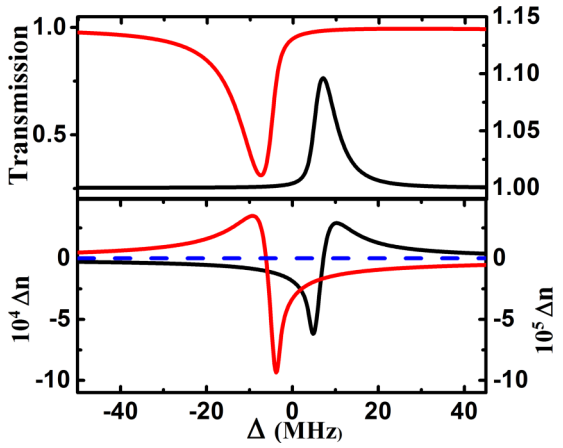

FIG. 2. Transmission and nonlinear refractive index (Δn) of the Stokes and anti-Stokes beams. The red solid line corresponds to the anti-Stokes beam and the black solid line corresponds to the Stokes beam. The scaling of the transmission and Δn for the anti-Stokes beams are presented in the left axis of the graph whereas that of the Stokes beam are presented in the right axis. The blue dotted line corresponds to the line of null refractive index.

while the real part contributes to the nonlinear refractive index as experienced by the generated fields. As for the case of the anti-Stokes beam, the roles of the pump and control beams are interchanged in the model. We calculated the transmission and nonlinear refractive index of the Stokes and anti-Stokes beams as presented in Fig. 2. The theoretical parameters are $\Omega_p = 60$ MHz, $\Omega_c = 140$ MHz, $\Delta_p = 1.2$ GHz, $\Delta_c = 800$ MHz, $v_p = 270$ m/s, and $N = 10^{13}/\text{cm}^3$. The model is verified by comparing with the experimentally measured transmission of an external probe beam coupling the system.

B. Wave-equations for the generated fields

The wave equation of the Stokes field propagating along the z direction with the radial transverse coordinate r is given as

$$\nabla^2 E_s(r) + \frac{\omega_s^2}{c^2}\left(1 + \chi_s^{(1)}\right)E_s(r) = \frac{-\omega_s^2}{\epsilon_0 c^2}P^{(NL)}(r),$$

$P^{(NL)}(r) = 3\epsilon_0\chi_{\text{XPM}}^{(\text{eff})}(r)E_s + 3\epsilon_0\chi_{\text{FWM}}^{(3)}E_pE_cE_a$ is the nonlinear polarization of the medium oscillating with frequency ω_s of the Stokes field, $\chi_{\text{FWM}}^{(3)}$ is the nonlinear susceptibility of the Stokes beam due to FWM and $\chi_s^{(1)}$ is the linear susceptibility, which is related to the linear refractive index as, $n_s = \sqrt{(1+\chi_s^{(1)})}$. We replace the electric field amplitudes in the propagation equation by, $E_i = A_i e^{\pm i n_i k_i z}$, $i = p, c, s, a$ with k_i being the wave vector and n_i being the linear refractive index associated with the corresponding field. With the slowly varying amplitude approximation, the wave equation now can be reduced to

$$i\frac{\partial A_s}{\partial z} + \frac{\nabla_T^2}{2k_s}A_s + i\alpha_s E_s + \frac{3}{2}k_s\text{Re}\left(\chi_{\text{XPM}}^{(\text{eff})}(r)\right)A_s + \frac{3}{2}k_s\chi_{\text{FWM}}^{(3)}A_pA_cA_a^*e^{i\Delta kz} = 0. \quad (2)$$

Here $\Delta k = n_pk_p - n_ck_c - n_sk_s + n_ak_a$ is the linear phase mismatch in the system. $\alpha_s = \frac{k_s}{2}\text{Im}(\chi_s^{(1)} + 3\chi_{\text{XPM}}^{(\text{eff})})$ accounts for the gain or absorption of the Stokes beam in the medium.

Due to the Gaussian profiles of the pump and the control fields, $\text{Re}(\chi_{\text{XPM}}^{(\text{eff})}(r))$ leads to the spatially varying nonlinear refractive indices $[\Delta n(r)]$ for the generated fields. $\Delta n(r)$ for the Stokes and the anti-Stokes fields are evaluated using the theoretical model for $r = 0$ and are presented in Figs. 3(a) and 3(d) as functions of the respective laser detunings. By energy conservation as discussed before, if δ_s is positive, then both the generated fields experience a positive nonlinear refractive index as specified by blue points in Figs. 3(a) and 3(d). $\Delta n(r)$ for the generated beams are found to be approximately Gaussian in nature leading to MOPO under the effect of the all-optical wave guide. The spatial modes of the generated fields under the effect of the all-optical waveguides can be studied using their propagation equations through the nonlinear medium. For the case of the lowest-order mode of the all-optical waveguides, the transverse sizes of the generated beams would be much smaller than that of the control and pump beams. In this case, the pump and the control fields can be considered as plane waves and hence the gain due to the four-wave mixing and the nonlinear absorption process would result in a uniform gain or loss in the transverse direction of the generated fields. Hence, it would be a good approximation to use that the spatial profiles of the generated fields are only decided by the optical waveguide while considering at least the lowest order mode. To determine the spatial mode of the generated field, only the nonlinear refractive index due to XPM is considered in Eq. (2) to get

$$i\frac{\partial A_{s,a}}{\partial z} = -\frac{1}{2k_{s,a}}\nabla_T^2 A_{s,a} + V_{s,a}(r)A_{s,a} = \beta_{s,a}A_{s,a}, \quad (3)$$

where $V_{s,a}(r) = -\Delta n_{s,a}(r)k_{s,a}$ are the near-Gaussian potentials as experienced by the Stokes and the anti-Stokes fields. The theoretically evaluated potentials are presented in Figs. 3(b) and 3(e) with parameters $\Omega_p = 30$ MHz, $\Omega_c = 140$ MHz for the pump and control beam sizes of 200 μm and 1 mm, respectively. The above equation (3) resemble the Schrödinger's equation for a two-dimensional Gaussian potential with eigenvalues $\beta_{s,a}$. We numerically solve the equations to find the eigenvalues of the potentials for both the generated beams, which are depicted as blue solid lines in Figs. 3(b) and 3(e). For efficient MOPO under the effect of an all-optical waveguide, the eigenmodes of the waveguide should meet the condition of complex phase-matching inside the medium as $(\beta_a - \beta_s + \Delta k) - i(\alpha_s - \alpha_a) = 0$. Apart from the phase-matching condition, a large overlapping integral is necessary for the efficiency of the process. To understand this, we consider the case of near-threshold MOPO. As depicted in Figs. 3(b) and 3(e), the waveguide for the Stokes beam has one spatial eigenmode whereas the anti-Stokes beam can support many eigenmodes. For both the waveguides, we plot the ground-state eigenfunctions and found them to be similar as shown in Figs. 3(c) and 3(f), which ensures a large overlapping integral.

If the generated fields are excited in one of the eigen modes of the waveguide, then the solution of the spatial modes would be $A_s = A_{s0}e^{i\beta_s z}$ and $A_a = A_{a0}e^{-i\beta_a z}$ for the

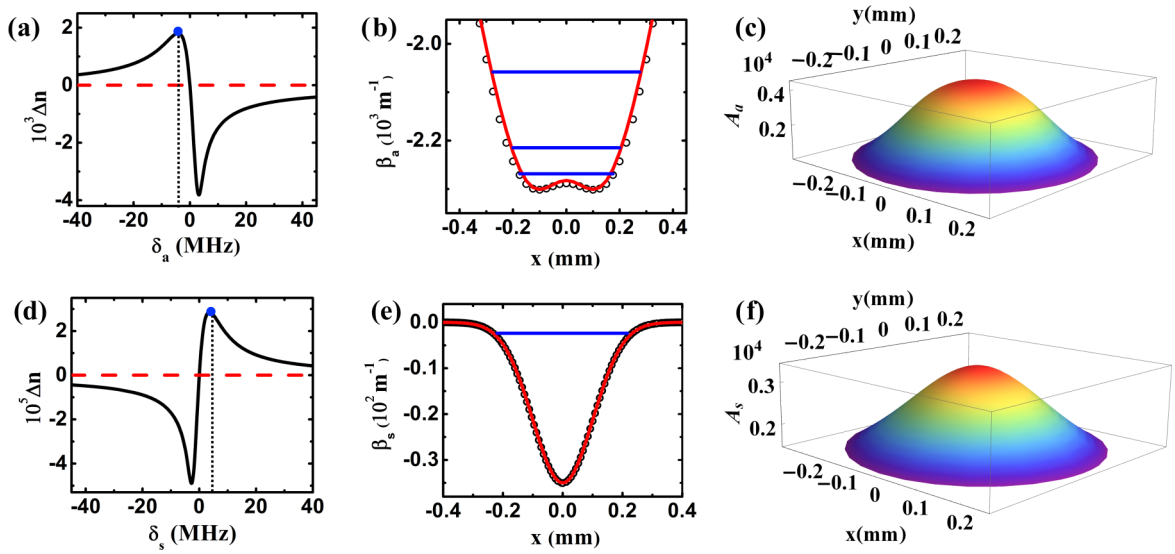

FIG. 3. Nonlinear refractive index (Δn) as a function of the two-photon detuning, (a) δ_a for anti-Stokes and (d) δ_s for Stokes fields. Transverse profile of the nonlinear refractive indices experienced by the generated fields due to Gaussian intensity profiles of the pump and control fields were calculated at specified points in the respective figures. Nearly Gaussian potentials experienced by (b) anti-Stokes and (e) Stokes fields. The black circles represent the potentials evaluated from the theoretical model and the red solid line signifies the functional fitting of the form $c_1(-e^{-x^2/(\Delta x_c)^2} + c_2 e^{-x^2/(\Delta x_p)^2})$ and $c_3(-e^{-x^2/(\Delta x_p)^2})$ for the anti-Stokes and Stokes beams, respectively, where $c_1 = 2.4 \times 10^3\,\mathrm{m}^{-1}$, $c_2 = 0.065$, $c_3 = 3.5 \times 10^2\,\mathrm{m}^{-1}$, $\Delta x_c = 680\,\mu$m and $\Delta x_p = 142\,\mu$m. The horizontal blue solid lines on the potentials denote the corresponding eigenvalues (theoretically calculated). The normalized ground-state eigenfunction of the waveguide for the case of (c) anti-Stokes field and (f) Stokes fields.

counterpropagating Stokes and anti-Stoke fields, respectively. Replacing the spatial mode solution in Eq. (1), we get

$$\frac{\partial A_{s0}}{\partial z} + \alpha_s A_{s0} = i\kappa_s A_{a0}^* e^{i(\beta_a - \beta_s + \Delta k)z},$$
$$-\frac{\partial A_{a0}}{\partial z} + \alpha_a A_{a0} = i\kappa_a A_{s0}^* e^{i(\beta_a - \beta_s + \Delta k)z},$$

where $\kappa_s = \frac{3}{2} k_s \chi^{(3)}_{\mathrm{FWM}} A_p A_c$ and $\kappa_a = \frac{3}{2} k_a \chi^{(3)}_{\mathrm{FWM}} A_p A_c$. These equations resemble the coupled equations for the Stokes and anti-Stokes fields in the undepleted strong field regime as presented in Refs. [6,11], which can be solved to calculate the threshold condition.

III. EXPERIMENTAL METHODS AND PRELIMINARY RESULTS

The schematic of the experimental setup and the relevant energy level diagram for the system are shown in Fig. 4(a). The experiment is performed with ^{85}Rb($D2$ line), where the pump laser is about 1.2 GHz blue-detuned to the transition $^5S_{1/2}$, $F = 2 \rightarrow 5P_{3/2}$, $F = 3$ and the control laser is detuned to the red of the transition $^5S_{1/2}$, $F = 3 \rightarrow 5P_{3/2}$, $F = 3$ by 800 MHz. The pump and control fields are passed through single mode fibers for mode cleaning and counterpropagate with each other through a 5-cm-long rubidium vapor cell housed inside two layers of magnetic shields. The temperature of the vapor cell is kept between 110°–120° C using a controlled heater which corresponds to a number density of approximately $10^{13}/\mathrm{cm}^3$. Both the strong fields are linearly polarized in the same direction and the generated fields are measured in the orthogonal polarization direction. 4-f imaging technique is used to image the generated beams at the respective exit-faces of the vapor cell. $\frac{1}{e}$ radii of the pump and the control beams used in the experiment are 200 μm and 1 mm, respectively. As a first observation of the signal, a Fabry-Perot cavity is used to measure the frequency difference between the generated Stokes and the pump beams. Figure 4(b) shows a typical cavity signal for near-threshold MOPO, where the small peak corresponds to a small leakage pump beam and the larger peak is due to the generated beam. With the free spectral range of the FPI being 1 GHz, the frequency difference of 35 MHz between the peaks confirms the generation of the Stokes beam being frequency-separated from the pump beam by the hyperfine difference of 3.035 GHz. The broad cavity signal is a result of mismatch of the cavity length (out of confocality). The pump threshold power is found to be 270 μW ($\Omega_p = 30$ MHz) when the control power is fixed at 54 mW ($\Omega_c = 140$ MHz). We observe that an increase in control power leads to the increase in the pump threshold power for the process, which is in accordance with the threshold condition derived in Ref. [11].

We experimentally investigate the multimode regime of the MOPO, which is observed for pump power far from the threshold value i.e. in the range, $\simeq$1.2–3.3 mW. We send a part of the Stokes beam into a fast photodetector, which is connected to a spectrum analyzer. In this regime, there is generation of at least two different temporal modes of the Stokes beams. These beams being the lower order modes of the waveguide, have beam waist of the order of 50 μm. With the experimentally measured beam power of $\simeq$150 μW, the corresponding Rabi frequency is as large as 100 MHz. Therefore, the beams undergo efficient forward four-wave mixing due to Zeeman degenerate two-level system [42]

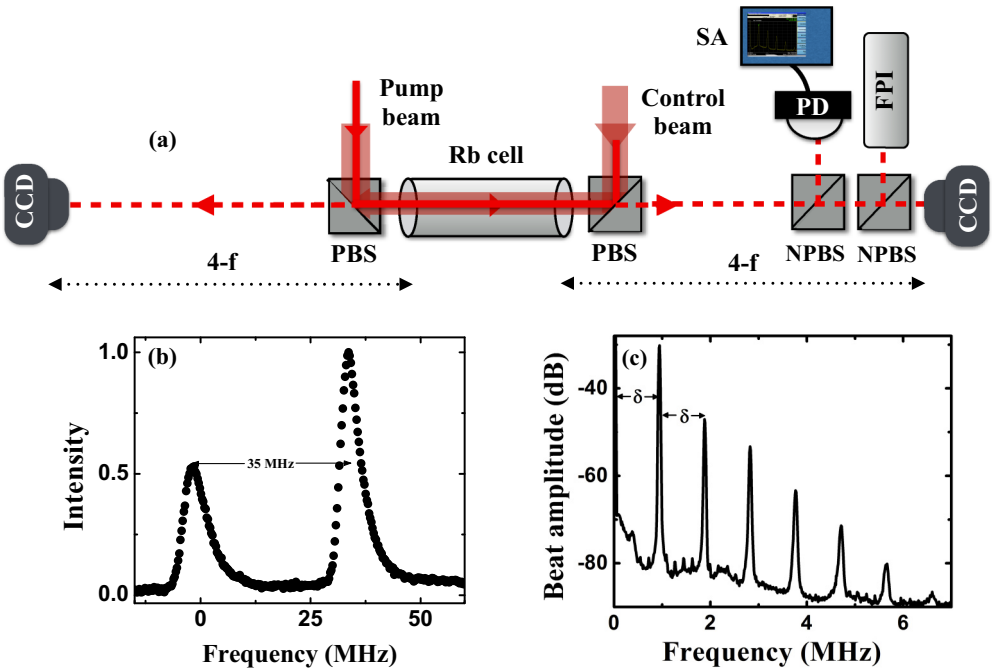

FIG. 4. (a) Schematic of experimental setup. (b) Cavity signal showing the frequency difference of about 35 MHz between the pump and the Stokes beam using a Fabri-Perot cavity of free spectral range of 1 GHz. (c) Spectrum analyzer signal showing the frequency comb under multispatial-mode regime.

and lead to the generation of equispaced frequency comb. Figure 4(c) depicts the spectrum analyzer signal showing the frequency comb with fundamental frequency δ. The value of δ can be tuned from hundreds of KHz to few MHz and strongly depends on the alignment of the strong driving beams as well as their Rabi frequencies and laser detunings. The same frequency comb structure is observed for the anti-Stokes beam simultaneously. Under certain parameter conditions, we observed multiple simultaneous frequency comb structures, which is due to the generation of three or more longitudinal modes. In this work, we focus on the single longitudinal mode regime of the MOPO to study the single spatial modes of the generated fields. This is experimentally verified by the fact that no frequency comb structure is observed for the single spatial modes.

IV. EXPERIMENTAL STUDY OF SINGLE SPATIAL MODE OF MOPO

The spatial profiles of the generated beams are imaged to the CCD camera at the exit faces of the vapor cell in both directions. The control beam power is kept fixed at 54 mW ($\Omega_c = 140$ MHz) and the transverse profiles of the Stokes and anti-Stokes beams are recorded by varying the pump beam power. We observe that with a very low pump power, i.e., $\simeq 270\,\mu$W ($\Omega_p = 30$ MHz), Stokes field with $54\,\mu$W is generated in the Gaussian spatial mode, which implies a pump conversion efficiency of $\sim$20%. The high efficiency is the consequence of the maximized overlapping integral due to the similar eigenfunctions of the Gaussian mode as presented in Figs. 3(c) and 3(f). In Figs. 5(a) and 5(b), we show the CCD images of the Gaussian mode and in Figs. 5(c) and 5(d), we show the corresponding intensity profiles along the transverse coordinate x for the Stokes and anti-Stokes beams, respectively. The different sizes for both the generated beams could be due to the fact that they are imaged at different positions of the cell, i.e., at the back face and front face of the cell for Stokes and anti-Stokes beam, respectively. Moreover, the control beam is 800 MHz red-detuned to the $^5S_{1/2}$,

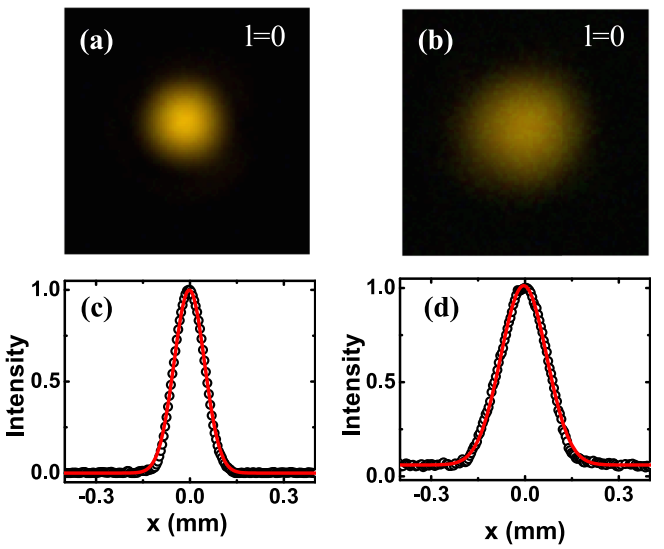

FIG. 5. CCD images of the symmetric Gaussian mode and the corresponding transverse intensity patterns in the generated (a), (c) Stokes and (b), (d) anti-Stokes fields, respectively. The intensity profiles are normalized to the peak value of intensities and are fitted with Gaussian distribution functions. The $\frac{1}{e}$ radii of the Gaussian Stokes and anti-Stokes beams are found to be 97 and 147 μm, respectively.

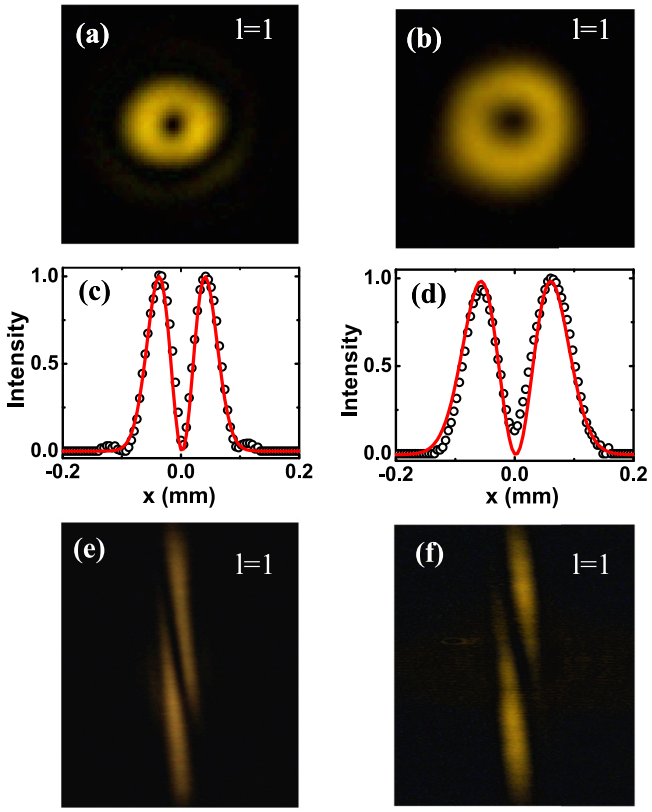

FIG. 6. CCD images of the first-order Laguerre-Gaussian (LG01) mode in the generated (a) Stokes and (b) anti-Stokes fields. The corresponding transverse intensity profiles for the (c) Stokes and (d) anti-Stokes fields. CCD images of the Laguerre-Gaussian (LG01) mode at the focal plane of the cylindrical lens for (e) Stokes and (f) anti-Stokes fields. The intensity profiles are normalized to the peak value of intensities and are fitted with Laguerre-Gaussian (LG01) distribution function. The $\frac{1}{e}$ radii of the Laguerre-Gaussian Stokes and anti-Stokes beams are found to be 55 and 83 μm, respectively.

$F = 3 \rightarrow {}^5P_{3/2}$, $F' = 4$ transition of ^{85}Rb, which falls within the Doppler width of ${}^5S_{1/2}$, $F = 2 \rightarrow {}^5P_{3/2}$, $F' = 3$ transition of ^{87}Rb and hence it is absorbed while propagating from the back face to front face of the cell. This makes the waveguiding potentials of the generated beams shallower leading to the larger radii of the generated beams on the front face of the cell.

In the same experimental setup, the Laguerre-Gaussian (LG) mode was achieved with a pump threshold power $\simeq$900 μW ($\Omega_p = 60$ MHz). Figures 6(a) and 6(b) refer to the corresponding CCD images where as Figs. 6(c) and 6(d) show the transverse intensity patterns for both the generated beams. In this case, we generate $\simeq$300 μW of Stokes power with 33% pump conversion efficiency. Furthermore, to confirm the phase singularity of the generated LG beams, we perform an additional measurement based on a method described in Ref. [43], i.e., by using a cylindrical lens in the path of each of the beams, where the transverse intensity pattern at the focal plane gives information about the orbital angular momentum of light. The CCD images at the focal plane of the cylindrical lenses for the Stokes and anti-Stokes fields as shown in Figs. 6(e) and 6(f) imply that both the beams are generated with same azimuthal index, i.e., $l = 1$ for this case. To understand this, we consider the overlapping integral, $\int_{-L/2}^{L/2}\int_0^R\int_0^{2\pi} \rho E_p^* E_c^* E_s E_{as} d\phi\, d\rho\, dz$ with L being the length of the sample; R being the aperture size of the system; z being the propagation direction; E_p, E_c, E_s, E_{as} being the electric field amplitudes of the pump, control, Stokes, and anti-Stokes fields, respectively. The integral over the azimuthal angle, $\int_0^{2\pi} e^{-i(l_s - l_{as})} d\phi = 2\pi\delta(l_s - l_{as})$ for counterpropagating Stokes and anti-Stokes fields. Hence both the generated LG beams are of same handedness whereas the selection for left or right-handedness depends mostly on the optical alignment of the input beams.

The excitation of single spatial mode of the generated LG beams can be understood by considering the pump depletion at the center of the beam due to the high conversion efficiency. This effect can modify the Gaussian Stokes potential by developing a bump at the center and simultaneously the anti-Stokes potential is modified in a similar fashion due to the cross phase modulation between the strong beams, e.g., as shown in Fig. 3(b). Hence we speculate that the overlapping integral for the lower Gaussian mode is minimized where as the potentials can favor the oscillation of the Laguerre-Gaussian mode with a better overlapping integral. However, a more accurate physical interpretation can be done by incorporating the effect of the depletion of the pump and the control fields in the wave equations for the generated fields. Taking the maximum overlapping of the generated beams into account for efficient generation, the beam sizes of both the beams should be similar inside the medium. Considering the LG (Gaussian) beam radius of 55 (97) μm at the back face of the cell as the beam waist, the free space propagation would have resulted in a beam radius of 236 (160) μm at the front face of the cell in the absence of waveguiding, which is larger than the measured beam radius of 83 (147) μm. This suggests that the beams are not diffracting over the vapor cell length (5 cm), which is larger than the Rayleigh range for the LG beams by a factor of $\simeq$4 and hence it confirms the presence of the all-optical waveguide in the system. Furthermore, we observed that the generated beams exhibit more confinement with higher input pump power in the single mode regime of MOPO. The beam waist of the generated LG mode (55 μm) at higher pump power (900 μW) is observed to be smaller as compared to the Gaussian mode (97 μm) generated at lower pump power (270 μW). This mode confinement is another evidence of the presence of waveguiding in the system. We also studied the free space propagation of the generated modes and the input fields after the vapor cell. We found that the size of the of the Stokes beam after free-space propagation distance of 5 cm is 340 μm, which is much larger than the size of the pump beam (210 μm). This suggests that the Stokes beam is confined within the pump beam inside the vapor cell. We further observed that the eigenfunctions differ more and more with higher-order modes and in turn leads to a reduction in MOPO process for the generation of higher-order spatial modes. As verified experimentally, the generation of the spatial modes, especially the higher-order modes are critical with regard to the beam sizes as well as the optical alignment of the strong driving fields.

As a further extension of the experiment, the symmetry of the waveguide potential along the transverse directions is

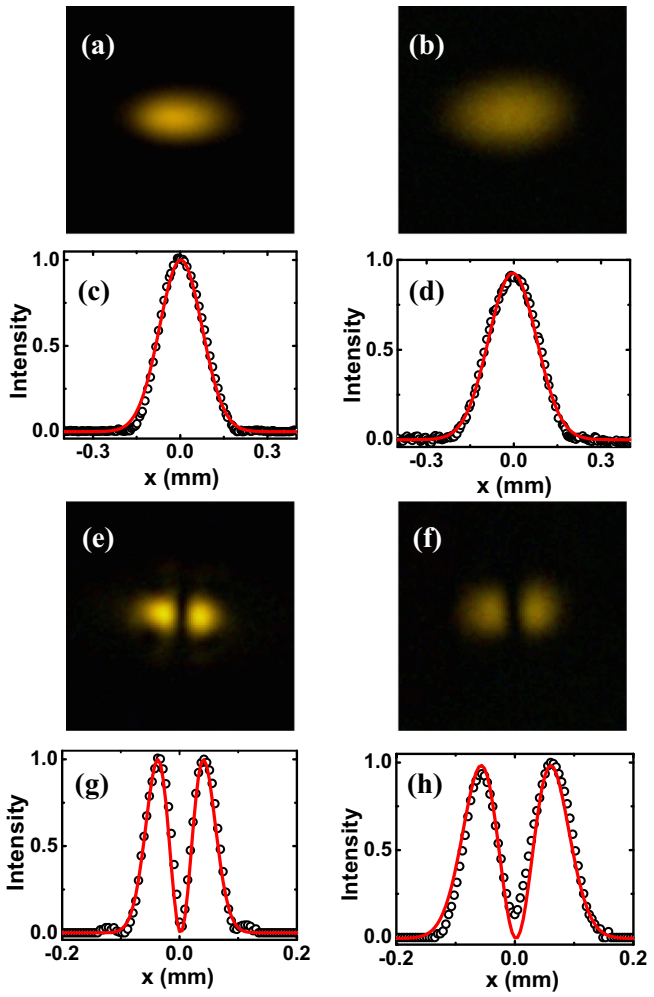

FIG. 7. CCD images of the asymmetric gaussian mode in the generated (a) Stokes and (b) anti-Stokes fields. The first-order Hermite-Gaussian (HG01) mode in the generated (e) Stokes and (f) anti-Stokes fields. The corresponding transverse intensity profiles are presented in (c), (d), (g) and (h) respectively.

broken by using an elliptical pump beam. A pair of anamorphic prisms are used to make the pump profile elliptic with ellipticity $\simeq$1.5. The same experiment is repeated to observe different spatial modes of the generated beams, i.e., by varying the pump power. The input asymmetric pump beam induces an asymmetric Gaussian potential for the generated fields and hence leads to the generation of asymmetric Gaussian mode near threshold as shown in Figs. 7(a) and 7(b). We fitted the intensity patterns along one transverse direction with Gaussian distribution function as a confirmation of the spatial mode, which is shown in Figs. 7(c) and 7(d). In this case, as the cylindrical symmetry of the waveguide is broken, the next higher-order eigenmode is the Hermite-Gauss mode. As expected, we observed the same mode in the experiment with an increase of the pump power. The corresponding CCD images presented in Figs. 7(e) and 7(f) and the intensity patterns along a transverse direction are shown in Figs. 7(g) and 7(h).

V. CONCLUSION

In this work, we studied the generation of all-optically guided MOPO which is found to be due to the combined effect of FWM and XPM in a system with efficient nonlinear processes. We report the generation of spatially as well as temporally correlated generated fields with a very high pump conversion efficiency. The maximum Stokes power observed in our experiment is $\sim$1mW with 30% pump conversion efficiency with suitable experimental parameters. Our further study includes optimization of the system to get stable higher order modes of the all-optical waveguide, study of the mechanism of the transition from single mode to multimode regime of the MOPO and study of the effect of the depletion in the pump and the control fields. Moreover, we plan to work on the mirrorless laser to increase its efficiency by feedback of the generated beam into the nonlinear medium. It would also be interesting to study the effect of the disorder introduced in the nonlinear refractive index experienced by the generated fields by using the random intensity pattern of the pump or control fields similar to the study of random lasers [44,45].

ACKNOWLEDGMENTS

The authors gratefully acknowledge useful discussions with Dr. T. N. Dey, D. Kara, A. Bhowmick, and T. Firdoshi. This work was financially supported by the Department of Atomic Energy, Government of India.

[1] S. E. Harris, Appl. Phys. Lett. **9**, 114 (1966).
[2] C. Canalias and V. S. Pasiskeviciu, Nat. Photon. **1**, 459 (2007).
[3] G. Strömqvist, V. Pasiskevicius, C. Canalias, and C. Montes, Phys. Rev. A **84**, 023825 (2011).
[4] G. Strömqvist, V. Pasiskevicius, C. Canalias, P. Aschieri, A. Picozzi, and C. Montes, J. Opt. Soc. Am. B **29**, 1194 (2012).
[5] C. Liljestrand, A. Zukauskas, V. Pasiskevicius, and C. Canalias, Opt. Lett. **32**, 2435 (2017).
[6] D. A. Braje, V. Balić, S. Goda, G. Y. Yin, and S. E. Harris, Phys. Rev. Lett. **93**, 183601 (2004).
[7] S. Du, J. Wen, and M. H. Rubin, J. Opt. Soc. Am. B **25**, C98 (2008).
[8] S. Du, P. Kolchin, C. Belthangady, G. Y. Yin, and S. E. Harris, Phys. Rev. Lett. **100**, 183603 (2008).
[9] V. Balić, D. A. Braje, P. Kolchin, G. Y. Yin, and S. E. Harris, Phys. Rev. Lett. **94**, 183601 (2005).
[10] P. Kolchin, Phys. Rev. A **75**, 033814 (2007).
[11] Y. Mei, X. Guo, L. Zhao, and S. Du, Phys. Rev. Lett. **119**, 150406 (2017).
[12] Y. Silberberg and I. B. Joseph, Phys. Rev. Lett. **48**, 1541 (1982).

[13] M. Pinard, D. Grandclement, and G. Grynberg, Europhys. Lett. **2**, 755 (1986).
[14] A. L. Gaeta, R. W. Boyd, J. R. Ackerhalt, and P. W. Milonni, Phys. Rev. Lett. **58**, 2432 (1987).
[15] G. Khitrova, J. F. Valley, and H. M. Gibbs, Phys. Rev. Lett. **60**, 1126 (1988).
[16] A. S. Zibrov, M. D. Lukin, and M. O. Scully, Phys. Rev. Lett. **83**, 4049 (1999).
[17] M. D. Lukin, P. R. Hemmer, M. Löffler, and M. O. Scully, Phys. Rev. Lett. **81**, 2675 (1998).
[18] M. Fleischhauer, M. D. Lukin, A. B. Matsko, and M. O. Scully, Phys. Rev. Lett. **84**, 3558 (2000).
[19] M. D. Lukin, A. B. Matsko, M. Fleischhauer, and M. O. Scully, Phys. Rev. Lett. **82**, 1847 (1999).
[20] W. Jiang, C. Han, P. Xue, L.-M. Duan, and G.-C. Guo, Phys. Rev. A **69**, 043819 (2004).
[21] C. H. R. Ooi, Q. Sun, M. S. Zubairy, and M. O. Scully, Phys. Rev. A **75**, 013820 (2007).
[22] K. Zhang, J. Guo, C.-H. Yuan, L. Q. Chen, C. Bian, B. Chen, Z. Y. Ou, and W. Zhang, Phys. Rev. A **89**, 063826 (2014).
[23] G. P. Agrawal, Phys. Rev. Lett. **64**, 2487 (1990).
[24] R. De La Fuente, A. Barthelemy, and C. Froehly, Opt. Lett. **16**, 793 (1991).
[25] G. A. Swartzlander, Jr. and C. T. Law, Phys. Rev. Lett. **69**, 2503 (1992).
[26] J. Cheng, S. Han, and Y. J. Yan, Phys. Rev. A **72**, 021801 (2005).
[27] A. André, M. Bajcsy, A. S. Zibrov, and M. D. Lukin, Phys. Rev. Lett. **94**, 063902 (2005).
[28] Q. Yang, J. T. Seo, B. Tabibi, and H. Wang, Phys. Rev. Lett. **95**, 063902 (2005).
[29] R. R. Moseley, S. Shepherd, D. J. Fulton, B. D. Sinclair, and M. H. Dunn, Phys. Rev. A **53**, 408 (1996).
[30] R. Kapoor and G. S. Agarwal, Phys. Rev. A **61**, 053818 (2000).
[31] H. Shpaisman, A. D. Wilson-Gordon, and H. Friedmann, Phys. Rev. A **71**, 043812 (2005).
[32] J. A. Andersen, M. E. J. Friese, A. G. Truscott, Z. Ficek, P. D. Drummond, N. R. Heckenberg, and H. Rubinsztein-Dunlop, Phys. Rev. A **63**, 023820 (2001).
[33] A. G. Truscott, M. E. J. Friese, N. R. Heckenberg, and H. Rubinsztein-Dunlop, Phys. Rev. Lett. **82**, 1438 (1999).
[34] P. K. Vudyasetu, D. J. Starling, and J. C. Howell, Phys. Rev. Lett. **102**, 123602 (2009).
[35] D. A. Akimov, E. E. Serebryannikov, A. M. Zheltikov, M. Schmitt, R. Maksimenka, W. Kiefer, K. V. Dukelskii, V. S. Shevandin, and Yu. N. Kondratev, Opt. Lett. **28**, 1948 (2003).
[36] O. Tzang, A. M. Caravaca-Aguirre, K. Wagner and R. Piestun, Nat. Photon. **12**, 368 (2018).
[37] S. Barreiro and J. W. R. Tabosa, Phys. Rev. Lett. **90**, 133001 (2003).
[38] G. Walker, A. S. Arnold, and S. Franke-Arnold, Phys. Rev. Lett. **108**, 243601 (2012).
[39] M. G. Bason, A. K. Mohaptra, K. J. Weatherill, and C. S. Adams, J. Phys. B **42**, 075503 (2009).
[40] K. Islam *et al.*, J. Phys. B **50**, 215401 (2017).
[41] O. N. Verma and T. N. Dey, Phys. Rev. A **91**, 013820 (2015).
[42] S. S. Sahoo, A. Bhowmick, and A. K. Mohapatra, J. Phys. B **50**, 055501 (2017).
[43] S. Alperin, R. Niederriter, J. Gopinath, and M. Siemens, Opt. Lett. **41**, 5019 (2016).
[44] D. S. Wiersma, Nat. Phys. **4**, 359 (2008).
[45] A. Schilke, C. Zimmermann, P. W. Courteille, and W. Guerin, Nat. Photon. **6**, 101 (2012).